The Astrophysical Journal, 774:5 (9pp), 2013 September 1 doi:10.1088/0004-637X/774/1/5

NEAR-INFRARED SPECTROSCOPY OF INFRARED-EXCESS STELLAR OBJECTS IN THE YOUNG SUPERNOVA REMNANT G54.1+0.3

Hyun-Jeong Kim[1], Bon-Chul Koo[1], and Dae-Sik Moon[2,3,4]
[1] Department of Physics and Astronomy, Seoul National University, Seoul 151-742, Korea; hjkim@astro.snu.ac.kr, koo@astro.snu.ac.kr
[2] Department of Astronomy and Astrophysics, University of Toronto, Toronto, ON M5S 3H4, Canada; moon@astro.utoronto.ca
[3] Space Radiation Laboratory, California Institute of Technology, Pasadena, CA 91125, USA
Received 2013 April 8; accepted 2013 June 11; published 2013 August 8

ABSTRACT

We present the results of broadband near-infrared spectroscopic observations of the recently discovered mysterious stellar objects in the young supernova remnant G54.1+0.3. These objects, which show significant mid-infrared-excess emission, are embedded in a diffuse loop structure of $\sim 1'$ in radius. Their near-infrared spectra reveal characteristics of late O- or early B-type stars with numerous H and He I absorption lines, and we classify their spectral types to be between O9 and B2 based on an empirical relation derived here between the equivalent widths of the H lines and stellar photospheric temperatures. The spectral types, combined with the results of spectral energy distribution fits, constrain the distance to the objects to be 6.0 ± 0.4 kpc. The photometric spectral types of the objects are consistent with those from the spectroscopic analyses, and the extinction distributions indicate a local enhancement of matter in the western part of the loop. If these objects originate via triggered formation by the progenitor star of G54.1+0.3, then their formations likely began during the later evolutionary stages of the progenitor, although a rather earlier formation may still be possible. If the objects and the progenitor belong to the same cluster of stars, then our results constrain the progenitor mass of G54.1+0.3 to be between 18 and $\sim 35\ M_{\odot}$ and suggest that G54.1+0.3 was either a Type IIP supernova or, with a relatively lower possibility, Type Ib/c from a binary system.

Key words: circumstellar matter – infrared: stars – ISM: individual objects (G54.1+0.3) – stars: early-type – techniques: spectroscopic

Online-only material: color figure

1. INTRODUCTION

Young core-collapse supernova remnants (SNRs), especially those with a connate pulsar, are usually rich in features useful for studying a diverse range of astrophysical problems. The very existence of a pulsar verifies the core-collapse nature of a progenitor star and limits the age of, and often distances to, an SNR, providing basic key information for better understanding of other relevant phenomena such as the evolution and dynamics of pulsar wind nebulae (PWNe) and supernova (SN) ejecta, distribution of circumstellar material from the mass loss of a progenitor, and shock interactions with the interstellar medium (ISM; e.g., Weisskopf et al. 2000; Gaensler et al. 2002; Moon et al. 2004, 2009; Koo et al. 2007; Lee et al. 2009). As we describe here, G54.1+0.3 is one such SNR that provides a unique opportunity for the in-depth study of either star formation triggered by an SN progenitor or the evolution of SN dust ejecta.

G54.1+0.3 is a young, core-collapse SNR with a central PWN that is prominent in synchrotron radio and X-ray emissions. As this SNR closely resembles the Crab Nebula, it is often referred to as a cousin of the Crab Nebula (Velusamy & Becker 1988; Lu et al. 2002). Its central pulsar (PSR J1930+1852), which is surrounded by a faint shell-like radio emission of $\sim 8'$ in diameter (Lang et al. 2010), has a 136 ms rotational period and a characteristic age of 2900 yr (Camilo et al. 2002; Lu et al. 2002). There is faint X-ray emission distributed along the inner boundary of the radio shell (Bocchino et al. 2010), and together the radio and X-ray morphologies strongly suggest that the emissions are from an SNR shell propagating into an ambient medium of an interstellar and/or circumstellar origin. Therefore, G54.1+0.3 belongs to a category of composite SNRs showing both a central PWN (or plerion) and a surrounding SNR shell. Notably, the recent detection of strong γ-ray emission from the SNR renders its PWN to be one with the highest γ-ray to X-ray luminosity ratios among all known PWNe driven by young rotation-powered pulsars (Acciari et al. 2010). H I and CO observations give the kinematic distance to G54.1+0.3 as 5–10 and 6–8 kpc, respectively (Koo et al. 2008; Leahy et al. 2008), while the dispersion measure of its central pulsar places the SNR at a distance of ~ 9 kpc (Cordes & Lazio 2002; see Section 3.3).

Interest in G54.1+0.3 has recently been sparked by the discovery of its diffuse infrared (IR) loop with a $\sim 1'$ radius (Koo et al. 2008). The IR loop, which was identified by observations using the *AKARI* satellite, consists of at least 11 embedded stellar objects with significant excess emission in the mid-infrared (MIR) wave bands; here, we refer to these as "IR-excess stellar objects." Their IR colors and spectral energy distributions (SEDs) are consistent with those of massive ($\gtrsim 10\ M_{\odot}$) pre-main-sequence (MS) stars with destroyed inner disks, which subsequently leads to the interpretation that their formation was triggered by a progenitor star of the SN in G54.1+0.3 (Koo et al. 2008). The *Spitzer* spectroscopy of the IR loop, however, implies that it is more likely made of freshly formed dust produced by the ejecta of the SN explosion and that the IR-excess stellar objects are in fact early-type MS stars of a stellar cluster to which the progenitor star originally belonged (Temim et al. 2010). Thus, it is imperative to carry out near-infrared (NIR) spectroscopic observations of the IR-excess stellar objects to

[4] Visiting Brain Pool Scholar, Korea Astronomy and Space Science Institute, Daejeon 305-348, Korea.

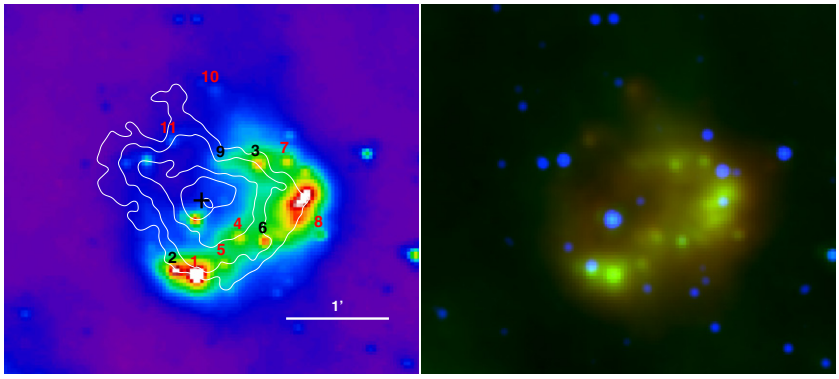

Figure 1. Left: *AKARI* 15 μm image of the SNR G54.1+0.3 and the 11 IR-excess stellar objects within the IR loop. The cross indicates the position of the pulsar at $(\alpha, \delta) = (19^{h}30^{m}30^{s}.13, +18^{\circ}52'14''.1$; J2000.0). The Very Large Array 4.85 GHz radio contours are also shown as an overlay. The contour levels are equally spaced every 1.28 K from 0.22 K in the brightness temperature and increase toward the center of the SNR. The numbers of the IR-excess stellar objects are in order of the *Spitzer* MIPS 24 μm brightness determined by point-spread function (PSF) photometry (Koo et al. 2008). Among them, the NIR spectra of seven objects marked with red were obtained in this study. The scale bar corresponds to 1′. North is up and east is to the left. Right: three-color image generated from the *Spitzer* IRAC 5.8 μm (B), the *AKARI* 15 μm (G), and the *Spitzer* MIPS 24 μm (R).

(A color version of this figure is available in the online journal.)

obtain more direct information for classifying the spectral types of the IR-excess stellar objects and, eventually, the origin of the IR loop.

In this paper, we present the results of an NIR spectroscopy study of the IR-excess stellar objects and discuss the implications of the results in the context of the two possible scenarios for their origin. The paper is organized as follows: in Section 2, we describe our observations and data reduction, followed by the spectral analyses and classifications as well as the distance determination in Section 3. In Section 4, we compare the results of the spectroscopic spectral classification with those from SED fit analyses and investigate the extinction distribution around the IR-excess stellar objects. We then discuss the origin of the IR-excess stellar objects in Section 5 and give our summary and conclusions in Section 6.

2. OBSERVATIONS AND DATA REDUCTION

2.1. Observations

NIR spectroscopic observations were performed for 7 of the 11 IR-excess stellar objects discovered by Koo et al. (2008) in the SNR G54.1+0.3 with the TripleSpec spectrograph on the 5 m Palomar Hale telescope on 2008 August 9. TripleSpec is a slit-based NIR cross-dispersion echelle spectrograph covering the entire NIR atmospheric window simultaneously with a spectral resolving power R of 2500–3000 using six (from 3 to 8) echelle orders mapped onto two adjacent quadrants of a Hawaii II HgCdTe 2 K × 2 K detector array from Teledyne, Inc. (Wilson et al. 2004; Herter et al. 2008). The slit width and length of TripleSpec are 1″ and 30″, respectively, and the broad spectral coverage of the spectrograph makes it ideal for conducting observations of new objects with little known information such as the IR-excess stellar objects in G54.1+0.3.

Figure 1 shows the positions of the IR-excess stellar objects in the *AKARI* 15 μm image numbered in decreasing order of their *Spitzer* MIPS 24 μm brightness (Koo et al. 2008). Table 1 lists the coordinates and magnitudes in the visible to MIR wave bands apart from those for Object 2, which has been detected only at $\lambda \gtrsim 3.6\,\mu$m (Monet et al. 2003; Zacharias et al. 2004; Koo et al. 2008). The photometric data used in Koo et al. (2008) are based on the *Spitzer* Infrared Array Camera (IRAC) Galactic Legacy Infrared Mid-Plane Survey Extraordinaire (GLIMPSE)[5] catalog, which somehow does not contain the Two Micron All Sky Survey (2MASS) NIR magnitudes of Object 6; these are instead obtained from the 2MASS All-Sky Point Source Catalog[6] (PSC; Skrutskie et al. 2006) and added in Table 1.

The seven objects (i.e., 1, 4, 5, 7, 8, 10, and 11) marked in red in Figure 1 were observed with TripleSpec in this work. However, the low signal-to-noise ratio (S/N) of Object 4, the faintest one in the K_s band, makes the reliable use of its spectrum difficult, and consequently, it has been excluded from further analysis. All the objects were observed with the typical AB nodding pattern, separated by 10″ along the slit direction, to effectively subtract the sky background emission. The total exposure time of each object was 600 s. The standard star HD 171623 (A0V) was observed at similar airmasses to those of the objects for standard star calibration.

2.2. Data Reduction

We first conduct flat fielding and bad pixel correction before obtaining two-dimensional wavelength solutions of the dispersed images using the OH sky emission lines. For each frame of a dithered pair, we subtract the sky background of a given frame using the other frame and then combine the pair of sky-subtracted spectra from the two frames to produce the final spectrum. Although TripleSpec covers wavelengths from 0.78 to 2.4 μm using six echelle orders of 3–8, we only use orders 3–6 (i.e., ∼1.0–2.4 μm) due to the low S/Ns of the spectra obtained in orders 7 and 8. The S/Ns of the final spectra range between 5 and 30. The extracted spectra show the features of the telluric absorption lines convolved with the TripleSpec system responsivity (Figures 2(a) and (d)).

For the standard source calibration, we are unable to find an appropriate standard spectrum of our calibration source HD 171623 (A0V) that can be used reliably to calibrate our TripleSpec spectra. Instead, we use the scaled model spectrum of Vega, which has the same spectral type and luminosity class as HD 171613, generated by the ATLAS12 stellar models (Castelli & Kurucz 1994) as the standard spectrum of our calibration source. The widths of the model H absorption lines of the

[5] http://www.astro.wisc.edu/glimpse/glimpsedata.html
[6] http://www.ipac.caltech.edu/2mass/releases/allsky

Table 1
Coordinates and Magnitudes of the IR-excess Stellar Objects in the SNR G54.1+0.3

Object	R.A. (J2000)	Decl. (J2000)	*B*	*V*	*R*	*I*	*J*	*H*	K_s	3.6	4.5	5.8	8.0	MIPS 24	MIPS 70	*AKARI* L15	*AKARI* L24
1	19:30:30.38	18:51:30.64	19.61	17.68	16.70	15.82	12.81	12.05	11.74	11.35	11.24	10.98	9.01	2.34	0.34	5.16	2.31
			0.50	0.50	0.50	0.50	0.02	0.03	0.02	0.03	0.04	0.05	0.03	0.06	0.33	0.05	0.06
2	19:30:31.29	18:51:32.81	...	...	...	...	...	...	...	12.41	12.04	11.39	9.70	3.40	0.45	5.85	3.12
			...	...	...	...	...	...	...	0.16	0.12	0.12	0.03	0.08	0.53	0.06	0.07
3	19:30:27.88	18:52:35.28	...	...	...	...	14.53	13.64	13.20	12.80	12.62	...	10.82	3.40	0.01	6.44	3.34
			...	...	...	...	0.04	0.03	0.04	0.05	0.07	...	0.05	0.08	0.41	0.06	0.07
4	19:30:28.61	18:51:52.37	...	...	17.86	17.06	13.93	13.09	12.71	12.30	12.24	12.14	11.64	3.43	0.46	6.94	3.51
			...	...	0.50	0.50	0.03	0.03	0.03	0.04	0.06	0.12	0.07	0.08	0.35	0.06	0.08
5	19:30:29.29	18:51:37.43	20.43	...	17.61	16.48	13.32	12.54	12.17	11.95	11.86	11.74	9.87	3.66	0.60	7.02	4.29
			0.50	...	0.50	0.50	0.02	0.02	0.02	0.04	0.05	0.08	0.03	0.07	0.75	0.07	0.08
6	19:30:27.58	18:51:50.31	...	...	...	...	13.61	12.75	12.11	11.47	11.08	10.73	9.60	3.74	0.25	6.40	4.16
			...	...	...	...	0.05	0.04	0.04	0.03	0.03	0.05	0.03	0.07	0.47	0.04	0.09
7	19:30:26.69	18:52:36.89	...	...	18.11	17.04	13.70	12.83	12.42	12.07	11.96	11.92	11.13	3.79	...	6.73	4.24
			...	...	0.50	0.50	0.03	0.03	0.03	0.04	0.05	0.07	0.05	0.09	...	0.06	0.14
8	19:30:25.29	18:51:53.69	19.92	...	16.66	15.76	13.40	12.61	12.25	12.01	11.80	11.86	11.06	3.99	0.22	7.24	4.16
			0.50	...	0.50	0.50	0.03	0.03	0.03	0.04	0.06	0.08	0.05	0.04	0.93	0.07	0.16
9	19:30:29.31	18:52:34.77	...	...	...	...	14.31	13.40	12.93	12.60	12.46	12.29	...	4.74	2.46	7.84	4.79
			...	...	...	...	0.03	0.03	0.03	0.05	0.06	0.10	...	0.09	4.35	0.10	0.09
10	19:30:29.72	18:53:18.27	20.50	...	18.14	16.87	13.65	12.84	12.50	12.22	12.15	11.92	11.98	5.33	2.39	8.86	5.06
			0.50	...	0.50	0.50	0.03	0.03	0.03	0.03	0.06	0.07	0.08	0.10	1.82	0.07	0.05
11	19:30:31.42	18:52:48.52	20.47	...	17.84	16.91	13.83	13.04	12.66	12.39	12.36	12.21	11.59	5.75	3.58	8.52	5.27
			0.50	...	0.50	0.50	0.03	0.04	0.04	0.03	0.06	0.09	0.06	0.10	2.92	0.06	0.04

Notes. The second rows list the magnitude errors (mag). The *BRI* magnitudes (Columns 4, 6, and 7) are from the USNO-B1.0 catalog (Monet et al. 2003), and the *V* magnitude (Column 5) is from the NOMAD catalog (Zacharias et al. 2004). The JHK_s magnitudes (Columns 8–10) and the IRAC magnitudes (Columns 11–14) are from the 2MASS All-Sky PSC and the GLIMPSE catalog, respectively. The *Spitzer* MIPS and *AKARI* MIR magnitudes are determined by PSF photometry (Koo et al. 2008).

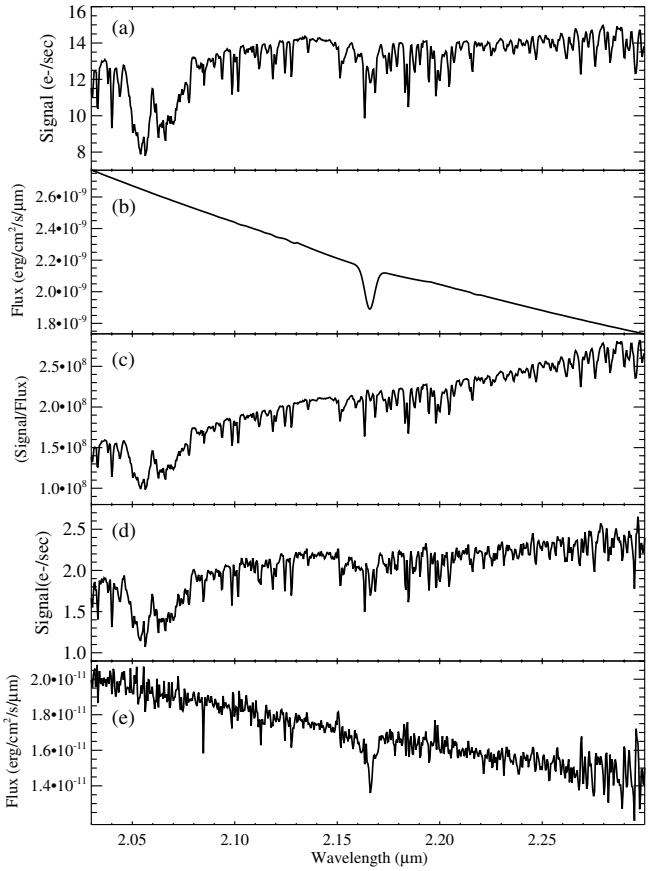

Figure 2. Standard star calibration process. (a) The observed spectrum of the standard star HD 171623. (b) The model spectrum of HD 171623. (c) The telluric line spectrum including the TripleSpec system responsivity obtained by dividing (a) by (b). (d) The observed spectrum of Object 1. (e) The final flux-calibrated spectrum of Object 1.

Vega spectrum are larger than those of the observed lines of HD 171623; therefore, we replace those lines, including Brγ, Br11, Br12, Paβ, and Paδ, with a Voigt profile in a scaled model spectrum if the lines do not blend or overlap. In the case where the H and telluric lines are adjacent (e.g., Brγ), the telluric lines are modeled using a Gaussian profile and subtracted.

Figure 2 presents an example of this calibration procedure for the order-3 (2.03–2.40 μm) spectrum of Object 1. The observed spectrum of the standard source HD 171623 in Figure 2(a) exhibits many telluric absorption lines and broad CO_2 absorption bands near 2.06 μm. This is divided by the model spectrum (Figure 2(b)) to produce the spectrum in Figure 2(c) featuring the telluric lines and system responsivity. The final calibrated spectrum (Figure 2(e)) is obtained by dividing the observed spectrum (Figure 2(d)) by the spectrum in Figure 2(c).

3. SPECTRAL TYPE CLASSIFICATION AND DISTANCE DETERMINATION

3.1. Near-infrared Spectra of Infrared-excess Stellar Objects

Figures 3 and 4 present the obtained spectra of the IR-excess stellar objects after normalization by a third- or fourth-order polynomial in wavelength ranges of 0.99–1.11, 1.22–1.31, 1.51–1.72, and 2.01–2.25 μm, corresponding to orders 6, 5, 4, and 3, respectively. Since higher orders have low throughputs for grating-based spectroscopy, the order-6 spectra have lower S/Ns than the others. Also note that the order-3 spectra are heavily contaminated by numerous telluric lines. For all the spectra, photospheric absorption lines are dominant; in particular, the H Brackett series are pronounced, including six continuous transitions of the Br11–16 series. In increasing order of the wavelength, we identify the following absorption lines: He I 1.003, Paδ 1.005, He I 1.083, He I 1.092, and

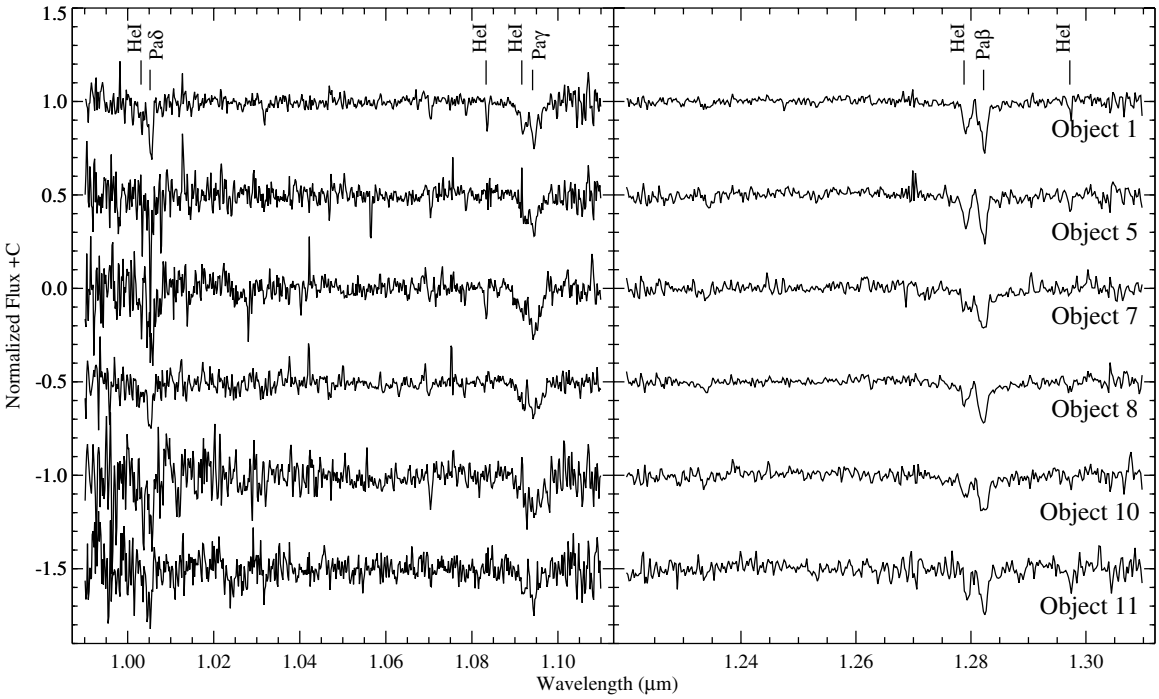

Figure 3. Orders 6 and 5 of the spectra of all the IR-excess stellar objects (Object 4 with a very low S/N is excluded). The spectra are normalized by a third- or fourth-order polynomial.

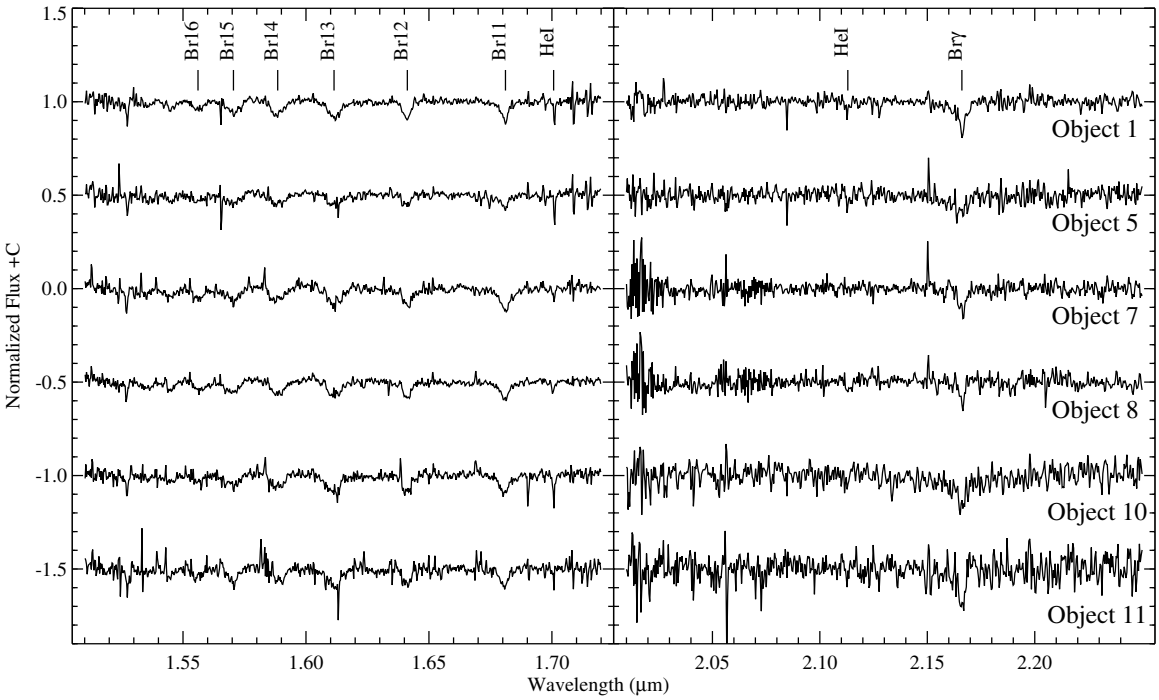

Figure 4. Same as Figure 3, but for orders 4 and 3.

Paγ 1.094 μm (order 6; Figure 3, left); He I 1.279, Paβ 1.282, and He I 1.297 μm (order 5; Figure 3, right); Br16 1.556, Br15 1.571, Br14 1.589, Br13 1.611, Br12 1.641, Br11 1.681, and He I 1.701 μm (order 4; Figure 4, left); and He I 2.113 and Brγ 2.166 μm (order 3; Figure 4, right).

We measure the equivalent widths (EWs) of the identified lines with a high S/N by fitting a Gaussian profile, and these results are presented in Table 2. Note that the EWs of the He I 1.297 μm line of Object 11, Br11 of Object 7, and Brγ of Object 5 are large because of contamination by nearby telluric features. In the obtained spectra shown in Figures 3 and 4, we have not identified any obvious emission lines. Some emission-like features in the spectra (e.g., those around $\sim$1.27 and $\sim$1.57 μm) are residuals of strong telluric lines that have not been completely removed during the standard star calibration.

3.2. Spectral Type Classification

The obtained spectra (Figures 3 and 4) of the IR-excess stellar objects show absorption lines of strong H transitions and relatively weak He I transitions. This, together with the lack of He II lines, indicates that these are stars of a late O- and early B-type between O8 and B3 (Hanson et al. 1996, 1998,

Table 2
Equivalent Widths of the Identified Lines

Object	He I (1.279 μm)	Paβ (1.282 μm)	He I (1.297 μm)	Br14 (1.589 μm)	Br13 (1.611 μm)	Br12 (1.641 μm)	Br11 (1.681 μm)	He I (1.701 μm)	He I (2.113 μm)	Brγ (2.166 μm)
1	2.13 ± 0.29	3.53 ± 0.30	0.77 ± 0.05	4.87 ± 0.82	5.36 ± 0.75	3.69 ± 0.55	3.39 ± 0.56	0.81 ± 0.25	1.19 ± 0.69	6.61 ± 1.21
5	2.10 ± 0.37	3.14 ± 0.38	0.56 ± 0.25	4.84 ± 1.57	3.24 ± 0.94	2.55 ± 0.73	1.77 ± 0.65	1.00 ± 0.30	0.78 ± 0.45	7.41 ± 1.80[a]
7	1.81 ± 0.53	3.91 ± 0.54	0.31 ± 0.28	6.39 ± 1.02	6.88 ± 0.82	3.70 ± 0.57	5.28 ± 0.69[a]	0.74 ± 0.30	0.51 ± 0.60	4.97 ± 1.13
8	1.54 ± 0.31	3.60 ± 0.34	0.60 ± 0.27	4.17 ± 0.60	5.82 ± 0.62	3.07 ± 0.41	3.97 ± 0.52	0.75 ± 0.25	1.80 ± 0.89	3.40 ± 0.89
10	1.47 ± 0.40	3.46 ± 0.46	0.35 ± 0.22	5.68 ± 1.06	6.30 ± 0.94	3.49 ± 0.63	4.14 ± 0.77	1.22 ± 0.30	1.29 ± 1.02	4.54 ± 1.44
11	1.77 ± 0.46	3.59 ± 0.56	1.29 ± 0.51[a]	5.83 ± 1.16	7.73 ± 1.14	2.97 ± 0.73	3.99 ± 0.85	0.79 ± 0.43	0.67 ± 0.80	6.26 ± 1.92

Notes. The central wavelengths are the vacuum wavelengths, and the EWs are in Å.
[a] Since these lines or the continuum of these lines are contaminated by telluric lines or noises, the equivalent widths of these lines might be measured larger than expected, so these values are upper limits.

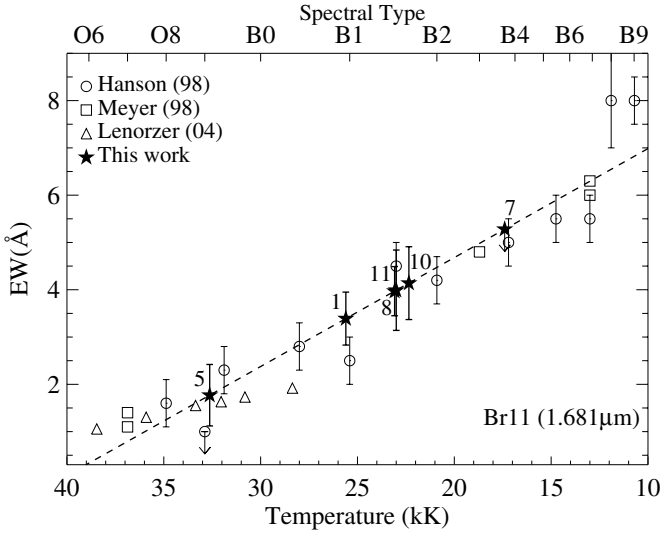

Figure 5. Relation between the EWs of Br11 and the stellar temperatures. Open circles, boxes, and triangles are from Hanson et al. (1998), Meyer et al. (1998), and Lenorzer et al. (2004), respectively. The dashed line is from a linear fitting of the EWs to the temperatures from Hanson et al. (1998; open circles). Filled stars show the positions of the six IR-excess stellar objects in this study on this relation.

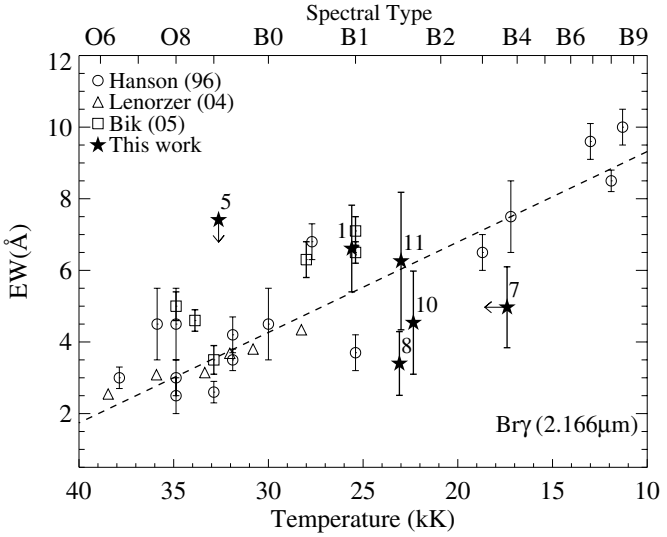

Figure 6. Same as Figure 5, but for Brγ. Open circles, triangles, and boxes are from Hanson et al. (1996), Lenorzer et al. (2004), and Bik et al. (2005), respectively. Filled stars are the IR-excess stellar objects of spectral types adopted from the results of Br11, i.e., determined by Equation (1). The dashed line is a linear fit of Hanson et al. (1996; open circles).

2005). This is consistent with the previous interpretation based on the *JHK*$_s$ color–color diagram and SEDs of these objects (Koo et al. 2008). Also, the absence of the He I 2.059 μm and Brγ emission lines suggests that they are MS stars rather than supergiants (Hanson et al. 1996).

To determine their spectral types more precisely, we first conduct a thorough literature search of reliable stellar spectroscopic libraries. However, as far as we are aware, only limited studies have been performed for NIR spectroscopic studies of OB stars so far, and even those available studies are somewhat inadequate for spectral classification use due to their small sample sizes (e.g., Wallace & Hinkle 1997; Meyer et al. 1998; Wallace et al. 2000) or paucity of the identified lines useful for line ratio comparison (e.g., Hanson et al. 1996, 1998, 2005; Bik et al. 2005).

The photospheric H lines of OB stars, on the other hand, are known to be very sensitive to temperature (Lenorzer et al. 2004), and, consequently, the EWs of the H lines are expected to be correlated with the stellar temperatures. Figure 5 confirms a correlation between the two parameters in the case of Br11, which exhibits a tight correlation (with a correlation coefficient of -0.94) of

$$\mathrm{EW_{Br11}\,(\text{Å})} = -0.23(\pm0.02) \times (T\,(\mathrm{kK})) + 9.29(\pm0.46). \quad (1)$$

Here, we use the results of Martins et al. (2005) and Schmidt-Kaler (1982) for the temperatures of OB stars and those of Hanson et al. (1998) for the line widths. The results of Meyer et al. (1998), which are based on much smaller sample sizes, also agree well with this relation. Note that among all the H lines in Table 2 Br11 is an ideal choice for this type of analysis because it is relatively well isolated and thereby free of contamination from nearby sky/telluric lines, although other photospheric H lines may be used for the same purpose as long as reliable measurements of their EWs are made. For instance, Figure 6 compares the temperatures of OB stars and the EWs of their Brγ lines available from Hanson et al. (1996), where the two parameters are still well correlated as

$$\mathrm{EW_{Br\gamma}\,(\text{Å})} = -0.25(\pm0.01) \times (T\,(\mathrm{kK})) + 11.84(\pm0.33). \quad (2)$$

The increased scatter in Figure 6 between the two parameters compared with that in Figure 5 is mainly caused by larger errors in the measured EWs of the Brγ lines, which are near telluric lines. The temperatures of the IR-excess stellar objects obtained using Equation (1) are presented in Table 3 along with their spectral types ranging between O9 and B2.

The uncertainties in the estimated temperatures of the IR-excess stellar objects in Table 3 (Column 2) represent those from the measurement errors of the EWs of the Br11 lines.

Table 3
Stellar Parameters Derived from the Relation between the Equivalent Widths of Br11 and the Stellar Temperatures

Object	Temperature[a] (K)	Spectral Type	Distance (kpc)	A_V (mag)
1	26000 ± 2000	B1 (B0.5–B1.5)	$4.6^{+0.4}_{-0.3}$	$7.4^{+\lesssim 0.05}_{-0.3}$
5	33000 ± 3000	O9 (O7.5–B0)	$8.1^{+1.9}_{-1.3}$	$7.5^{+\lesssim 0.05}_{-0.1}$
7	$\gtrsim 17000$	$\lesssim$ B3.5	$\gtrsim 3.3$	$\gtrsim 7.8$
8	23000 ± 2000	B1.5 (B1–B2)	$5.4^{+0.5}_{-0.7}$	$6.9^{+0.1}_{-\lesssim 0.05}$
10	22000 ± 3000	B2 (B1–B3)	$5.5^{+0.9}_{-1.2}$	$7.4^{+0.1}_{-0.2}$
11	23000 ± 4000	B1.5 (B1–B2.5)	$6.5^{+1.2}_{-1.7}$	$7.1^{+0.2}_{-0.2}$

Note. [a] The effective temperatures of the MS stars are adopted from Martins et al. (2005) for O-type stars and those of Schmidt-Kaler (1982) for stars later than B0.

The scatter in the correlation between the EWs and the stellar temperatures in Equation (1) is an additional source of uncertainty of ~2000 K. The combined uncertainties of these two are roughly equivalent to one subclass in the determined spectral types (Column 3) of the IR-excess stellar objects. Furthermore, there is an intrinsic difference of approximately one spectral subclass around the late O and early B spectral types between the two stellar models of Martins et al. (2005) and Schmidt-Kaler (1982). We therefore believe that the spectral types of the IR-excess stellar objects in Table 3 have uncertainties equal to a total of two subclasses.

It is notable that the measured EWs (~1 Å) of the He I lines (Table 2) are also consistent with the interpretation that the spectral types of the IR-excess stellar objects lie between late O- and early B-type stars (see Hanson et al. 1996, 1998 for details).

3.3. Distance Determination

We estimate the photometric distance to the six IR-excess stellar objects based on the determined temperatures by fitting their SEDs with the ATLAS9 Kurucz stellar models (Castelli & Kurucz 2003). For this, we use wavelengths shorter than 5 μm in the SED fits, to concentrate on stellar emission, and the interstellar reddening law of $R_V = 3.1$ (Draine 2003). The best-fit distances and extinctions lie within 3.3–8.1 kpc and A_V = 6.9–7.8 mag, respectively, with mean values of 6.0 ± 0.4 kpc and 7.3 ± 0.1 mag (Table 3).

Figure 7 shows the distribution of the obtained distances and extinctions. The two parameters of Object 7 only have lower limits because the lack of a *B*-band magnitude makes it difficult to determine the upper limits—note that the *B*-band magnitude is critical in determining the temperature of OB-type stars in the SED fits. The large extinction ($A_V \gtrsim 7.8$ mag) together with the absence of the *B*-band magnitude indicates that Object 7 has a locally increased extinction. We discuss the extinction of the IR-excess stellar objects in Section 4.

The distance to G54.1+0.3 was previously determined in several studies to be 5–10 kpc based on 21 cm H I absorption lines (Koo et al. 2008; Leahy et al. 2008) and $9^{+1.0}_{-1.5}$ kpc from a dispersion measure analysis of the central pulsar J1930+1852 (Camilo et al. 2002; Cordes & Lazio 2002). Two additional distances of 8 kpc and $6.2^{+1.0}_{-0.6}$ kpc have been proposed from ^{13}CO $J = 1$–0 observations of nearby molecular clouds (Koo et al. 2008; Leahy et al. 2008), although it is uncertain whether the clouds are indeed associated with the SNR (Lee et al. 2012).

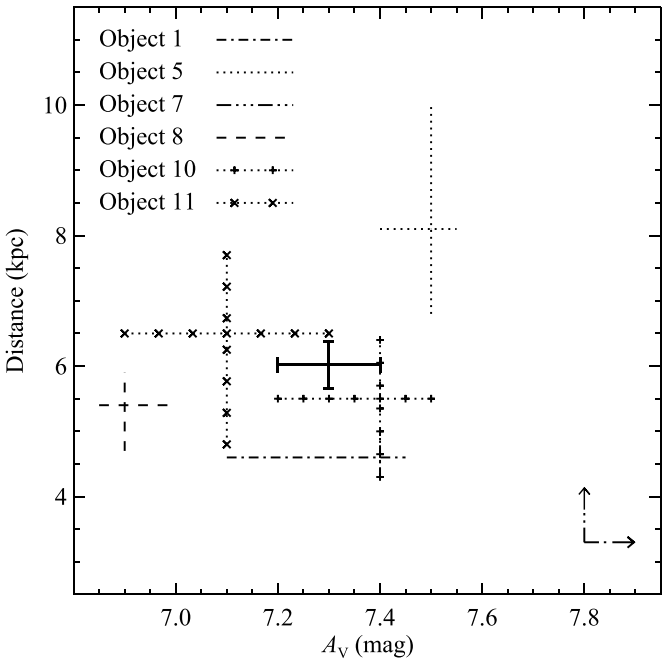

Figure 7. Distances and extinctions to the individual IR-excess stellar objects derived from the SED fitting with the upper and lower temperature limits determined by Equation (1). The mean distance 6.0 ± 0.4 kpc and mean extinction $A_V = 7.3 \pm 0.1$ mag are shown as solid lines. Object 7 only gives lower limits (see Section 3.3).

The 6.0 ± 0.4 kpc distance to the IR-excess stellar objects derived from the SED fits in this study is somewhat smaller but still consistent with previously reported values. Since our result is independent of the Galactic rotation model, we adopt 6 kpc as the distance to both the IR-excess stellar objects and G54.1+0.3 in the following discussion.

4. PHOTOMETRIC SPECTRAL CLASSIFICATION AND EXTINCTION DISTRIBUTION

As we have shown, the spectral features of the six observed IR-excess stellar objects in the IR loop of the SNR G54.1+0.3 indicate that they are late O- or early B-type stars, which is consistent with the previous interpretation based on their JHK_s colors (Koo et al. 2008). Given the importance of the spectral classification of the IR-excess stellar objects (see Sections 1 and 5) in understanding their nature in association with G54.1+0.3, it is worthwhile obtaining spectral classifications of the remaining five objects, i.e., Objects 2, 3, 4, 6, and 9. For this, we again fit SEDs in the ~0.4–5 μm range of all the IR-excess stellar objects using the ATLAS9 Kurucz stellar models (Castelli & Kurucz 2003). We fix the distance to 6 kpc (as determined in Section 3.3) and derive the best-fit temperatures and extinctions, which allows us to obtain photometric spectral classifications of these five objects lacking NIR spectroscopic information. For the other six objects classified using the NIR spectra (Section 3.2), the SED fits provide us with confirmation that the derived spectral types are correct. Object 2, however, is excluded from the SED fits because it is detected only at longer ($\gtrsim 3$ μm) wave bands. (Our most recent observations reveal that this object is composed of two sources (H.-J. Kim et al., in preparation).)

A comparison of the observed and best-fit SEDs of all the IR-excess stellar objects other than Object 2 is presented in Figure 8. We note that the observed *R*-band fluxes of Objects

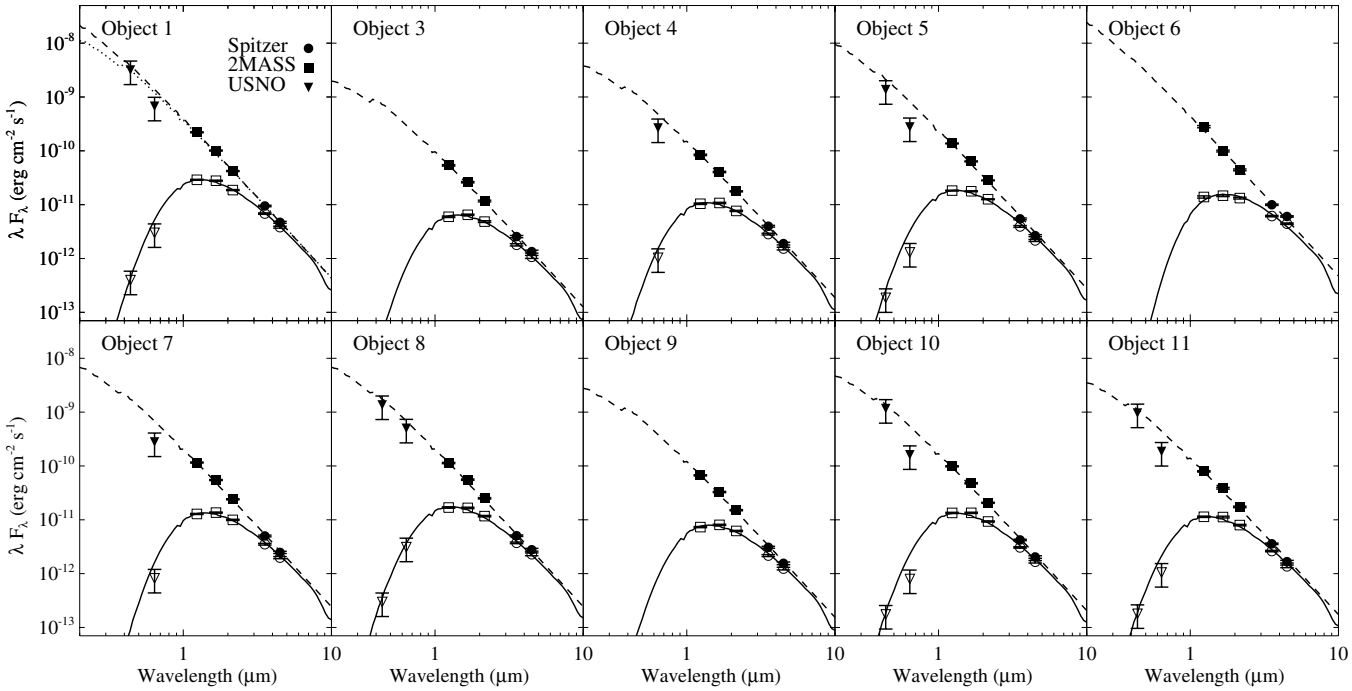

Figure 8. Observed and best-fit SEDs of the IR-excess stellar objects. The open symbols and solid lines represent the observed and fitted SEDs, respectively, and the filled symbols and dashed lines are those for the extinction-corrected values adopting the interstellar reddening law of $R_V = 3.1$ (Draine 2003). The dotted line of Object 1 is a model SED assuming a binary system comprising two early-type stars of $T = 24{,}000$ K (see Section 4). Object 2, which does not have enough data points, is excluded from the fitting.

Table 4
Spectral Types and Extinctions Derived in the SED Fits Using Photometric Observations with Fixed Distance of 6 kpc

Object	Temperature[a,b] (K)	Spectral Type	A_V (mag)	χ^2_{red}
1	32000	O9.5	7.4 ± 0.1	2.7
2	...	...	...	...
3	20000	B2.5	8.0 ± 0.2	2.3
4	23000	B1.5	7.6 ± 0.2	3.0
5	27000	B0.5	7.4 ± 0.1	13.0
6	33000	O9	11.0 ± 0.2	11.0
7	25000	B1	8.0 ± 0.1	6.8
8	26000	B1	7.0 ± 0.2	4.0
9	21000	B2	8.1 ± 0.2	6.6
10	24000	B1.5	7.3 ± 0.1	12.2
11	22000	B2	7.1 ± 0.1	6.0

Notes.
[a] The effective temperatures of the MS stars are adopted from Martins et al. (2005) for O-type stars and those of Schmidt-Kaler (1982) for stars later than B0.
[b] The 1σ uncertainty of temperature is less than temperature interval in the fitting.

5, 10, and 11 are somewhat lower than expected from the model calculations. The origin of these discrepancies in the *R* band is not clear, although the slightly loose photometric calibration in the USNO-B1.0 catalog and/or the conversion between the USNO photographic magnitude system (Monet et al. 2003) and the standard Johnson–Cousin system may be responsible. Table 4 contains the resulting best-fit parameters derived in the SED fits with their reduced χ^2 values. The spectral types are taken from models of Martins et al. (2005; for O-type stars) and Schmidt-Kaler (1982; for B-type stars), which are mapped to the best-fit temperatures of the Kurucz models. All the IR-excess stellar objects are early-type stars of similar spectral type between O9 and B2.5, which is consistent with the previous results from their JHK_s colors and also with the results from the NIR spectral analyses.

The best-fit SED temperatures of the IR-excess stellar objects in Table 4 are similar to those derived from the EWs of their NIR absorption lines (Section 3.2), except for those of Objects 1 and 5 which show relatively large discrepancies: 26,000 K (from the EWs) in contrast to 32,000 K (from the SED fits) for Object 1, and 33,000 K (from the EWs) in contrast to 27,000 K (from the SED fits) for Object 5. As we explain in Section 3.2, we consider this temperature difference of ~6000 K, which is roughly equivalent to two spectral subclasses, to lie within the uncertainty range inherent in the classification of the spectral types of the IR-excess stellar objects. Comparing Objects 1 and 5, however, we note that the former has stronger H absorption lines, which would indicate a lower temperature (Figures 3 and 4), even though it has a higher SED temperature (Figure 8 and Table 4). One possible explanation for this is that Object 1 is a binary system of two early-type stars, similar to Object 2. The dotted line of Object 1 in Figure 8 shows such an example where we calculate the expected SED of a binary system comprising two early-type stars of $T = 24{,}000$ K.

Table 4 also contains the extinctions of the IR-excess stellar objects, where the six objects (1, 5, 7, 8, 10, and 11) with the obtained NIR spectra show almost identical extinctions to those in Table 3. The extinctions of all the IR-excess stellar objects are between $A_V = 7$ and $A_V = 11$ mag, and Objects 3, 4, 6, 7, and 9, which have extinctions of $A_V \gtrsim 8.0$ mag, appear to be located in the western part of the IR loop (Figure 1). This is consistent with their relative faintness as listed in Table 1 and their non-detection in the *B* band, which is the most sensitive to increased extinctions. The increased extinctions indicate a potential enhancement of matter in the western part of the IR loop, and the relatively smaller (A_V ~7 mag) extinctions of the

objects in the outer part of the loop, i.e., Objects 8, 10, and 11, support this interpretation.

Lu et al. (2002) previously estimated the average X-ray absorption column density toward the central pulsar in G54.1+0.3 to be $N(\mathrm{H}) = (1.6 \pm 0.1) \times 10^{22}$ cm^{-2} (or $A_V = 8.4 \pm 0.5$ mag), whereas in the deeper X-ray observations of Temim et al. (2010), a spatial variation in the absorption column density with a mean value of $N(\mathrm{H}) = (1.95 \pm 0.04) \times 10^{22}$ cm^{-2} (or $A_V = 10.2 \pm 0.2$ mag) was found. The extinction values estimated from the X-ray observations are somewhat larger than those of the IR-excess stellar objects from the SED fits in this study, which suggests the possibility of a much wider dust distribution than the observed IR loop, e.g., a shell-like distribution surrounding the X-ray PWN of G54.1+0.3 that is invisible due to the absence of heating sources.

5. DISCUSSION

Two possible scenarios that explain the relation between the IR-excess stellar objects and the SNR G54.1+0.3 have been proposed: (1) Koo et al. (2008) proposed that the IR-excess stellar objects are massive young stellar objects (YSOs) whose formation was triggered by the progenitor of G54.1+0.3 based on their SEDs and spatial confinement to the IR loop; and (2) Temim et al. (2010), using the results obtained with *Spitzer* IRS observations, proposed that the IR-excess stellar objects are members of a stellar cluster to which the progenitor of the SNR originally belonged and that the IR emission is from the ejecta dust heated by the stellar objects. We discuss these two scenarios in the context of the results presented in this paper.

5.1. Young Stellar Objects Triggered by the Progenitor Star

In the first scenario, the IR-excess stellar objects are interpreted to be massive YSOs whose formation was triggered by the progenitor of the SNR G54.1+0.3 (Koo et al. 2008). As Koo et al. (2008) have previously shown, the SEDs of the IR-excess stellar objects have a dip at around 8 μm with a strong MIR excess, similar to those of stars without substantial circumstellar material such as YSOs with a truncated disk or Herbig Ae/Be stars with a breakup inner disk (Hillenbrand et al. 1992; Malfait et al. 1998; D'Alessio et al. 2005). However, the NIR spectra (Figures 3 and 4) of the IR-excess stellar objects do not show any emission lines that are often found in Herbig Ae/Be stars (Hillenbrand et al. 1992; Malfait et al. 1998). This indicates that the IR-excess stellar objects are in a relatively later evolutionary stage of pre-MS stars with only little nearby circumstellar material remaining. In general, the disk lifetime of YSOs is well correlated with the mass of the central star, and for stars more massive than 7 $M_\odot$, it is known that disk dispersion takes less than 1 Myr (Hillenbrand et al. 1992; Alonso-Albi et al. 2009). Hence, the IR-excess stellar objects are likely to be a few million years old, and their formation may have been triggered during the late MS or post-MS evolutionary stages of the progenitor. In the case of the latter, a potential delay in the triggered formation process due to local environment effects has been proposed (Koo et al. 2008).

The IR loop in G54.1+0.3, where the IR-excess stellar objects are embedded, was suggested to be composed of fast-expanding SN ejecta dust (Temim et al. 2010), although this does not preclude the existence of the local ISM and/or circumstellar material in the loop. If the ejecta dust is illuminated by the IR-excess stellar objects, then significant enhancement of the MIR emission can occur, and depending on the distance between the two, the 8 μm dip features seen in the SEDs of the latter (Figure 8) may arise. If the IR emission of the stellar objects is from SN dust rather than circumstellar dust, then the IR-excess stellar objects would be older than a few million years, and subsequently, the triggered formation by the progenitor star of G54.1+0.3 could have happened earlier, e.g., during their MS stages.

On the other hand, we note that confirmation of the IR-excess stellar objects as a result of triggered star formation is somewhat uncertain based on the available information from the existing observations. As described above, the spatial confinement of the IR-excess stellar objects in the IR loop surrounding the PWN in G54.1+0.3 indicates potential triggered star formation by the SN progenitor star. However, recent numerical simulations of the feedback effects on star formation (Dale & Bonnell 2011; Dale et al. 2012) suggest that the features such as bubble walls or pillars, in which young stars are embedded, do not always trace triggered star formation, although they may serve as a good indicator. According to the results, such geometrical distributions of stars can be produced without feedback, depending on environments (Dale & Bonnell 2011; Dale et al. 2012).

5.2. Stellar Cluster Origin

According to the second scenario, an SN exploded as a member of a cluster of stars that includes the IR-excess stellar objects, and the stellar cluster illuminates the SN ejecta dust to produce the strong MIR emission that is observed (Temim et al. 2010). In this case, the results of the NIR spectroscopy reported in this paper help constrain the mass and type of the SN progenitor as follows. First, the mass ($M \sim 17\ M_\odot$) of an O9 star, which is the earliest spectral type of the IR-excess stellar objects (Table 4), gives the lower limit of the progenitor mass, and considering the continuous distribution of the initial mass function (e.g., Salpeter 1955), the progenitor mass cannot be much greater than that of an O9 star. In other words, it is unlikely that the progenitor was massive enough to be a Wolf–Rayet star of $\gtrsim$35 $M_\odot$ (e.g., Smith et al. 2011 and the references therein). Consequently, we can constrain the progenitor mass to be in the range of 18–35 $M_\odot$, although the upper limit may be significantly lower than 35 $M_\odot$.

The SN type of G54.1+0.3 has not yet been definitively confirmed. Chevalier (2005) previously ruled out the IIL/b possibility due to a lack of any observational evidence indicating the existence of strong circumstellar interactions and suggested that G54.1+0.3 is an SN IIP or Ib/c. If the progenitor star was a single star, then we believe that it is less likely to be an SN Ib/c, given the upper mass limit, which leaves us only with the IIP possibility. The mass range of SN IIP progenitors was first calculated to be 9–25 $M_\odot$ by Heger et al. (2003) based only on single star evolutionary models. Smith et al. (2011), however, recently suggested a smaller range of 8–18 $M_\odot$ after observationally accounting for contributions from both single stars and binaries in the entire core-collapse populations. This range of Smith et al. (2011) for the progenitor mass of SNe IIP places the G54.1+0.3 progenitor mass close to the upper limit, similar to that of the O9 star, which is the earliest existing member of the cluster as noted. Therefore, if the progenitor of G54.1+0.3 was indeed a member of the cluster to which the IR-excess stellar objects also belong and exploded as an SN IIP, the spectral type of the progenitor should be that of a late O-type star (e.g., O8). Finally, we note that in principle we cannot yet completely rule out the possibility of the G54.1+0.3 progenitor

being a binary that exploded as an SN Ib/c, although we believe that this possibility is low since SNe Ib/c from binaries are much less abundant than SNe IIP.

6. SUMMARY AND CONCLUSIONS

We present the results of broadband NIR spectroscopic observations and SED analyses of the IR-excess stellar objects discovered in the IR loop of the SNR G54.1+0.3. A summary of our results and main conclusions is below.

1. We spectroscopically determine the spectral types of the six IR-excess stellar objects to be between O9 and B2 based on the empirical relation (see Equation (1)) between the EWs of the H lines and stellar temperatures that we establish using the results of previous studies available in the literature. The determined spectral types are consistent with those from the JHK_s color analyses. The established relation between the EWs of the H lines and stellar temperatures can generally be used to determine the spectral types of OB stars with NIR spectra, and it is worthwhile to refine the relation in the future by increasing the sample size.
2. We determine the distance, which is independent of the Galactic rotation model, to the IR-excess stellar objects to be 6.0 ± 0.4 kpc based on our SED fits. The distance of 6 kpc is somewhat smaller than but still compatible to the previously proposed distances to G54.1+0.3.
3. The photometric spectral types of most of the IR-excess stellar objects lie within the range of O9–B2.5, which is consistent with the spectroscopic results. The extinctions of the IR-excess stellar objects, with a mean of $A_V = 7.9 \pm 0.1$ mag, increase in the western part of the IR loop, indicating an enhancement of matter in that region.
4. If the formation of the IR-excess stellar objects was triggered by the progenitor star of G54.1+0.3, then the lack of emission lines in our NIR spectra indicates that the objects are likely to be a few million years old, which is suggestive of triggering occurring during the late MS or post-MS stages of the progenitor. However, the potential contributions of the SN ejecta dust to the observed MIR emission of the IR-excess stellar objects may also be consistent with triggering during the MS stages.
5. If the IR-excess stellar objects are members of a stellar cluster to which the progenitor originally belonged, then our NIR spectroscopic results constrain the mass of the progenitor to be slightly greater than 17 $M_\odot$. In such a case, it is more likely that G54.1+0.3 was an SN IIP.

The NIR spectroscopic observations of the IR-excess stellar objects in the SNR G54.1+0.3 presented in this study provide important information about their nature, particularly the spectral types. However, their origin and relation with the SNR are still unclear. Further investigations on the dust in the IR loop and the progenitor of G54.1+0.3, accompanied by the use of physical models, will help decipher the nature of the IR-excess stellar objects and substantiate a more plausible scenario of their origin.

This publication makes use of data products from the Two Micron All Sky Survey, which is a joint project of the University of Massachusetts and the Infrared Processing and Analysis Center/California Institute of Technology, funded by the National Aeronautics and Space Administration and the National Science Foundation. This work was supported by NRF (National Research Foundation of Korea) Grant funded by the Korean Government (NRF-2012-Fostering Core Leaders of the Future Basic Science Program). B.-C.K. is supported by Basic Science Research program through the National Research Foundation of Korea (NRF) funded by the Ministry of Education, Science, and Technology (NRF-2011-0007223). D.-S.M. acknowledges support from the Natural Science and Engineering Research Council of Canada. This paper was studied with the support of the Ministry of Education, Science, and Technology (MEST) and the Korean Federation of Science and Technology Societies (KOFST). We thank Professor Sang-Gak Lee for helpful advice on calibration and analysis of TripleSpec spectra.

REFERENCES

Acciari, V. A., Aliu, E., Arlen, T., et al. 2010, ApJL, 719, L69
Alonso-Albi, T., Fuente, A., Bachiller, R., et al. 2009, A&A, 497, 117
Bik, A., Kaper, L., Hanson, M. M., & Smits, M. 2005, A&A, 440, 121
Bocchino, F., Bandiera, R., & Gelfand, J. 2010, A&A, 520, A71
Camilo, F., Lorimer, D. R., Bhat, N. D. R., et al. 2002, ApJL, 574, L71
Castelli, F., & Kurucz, R. L. 1994, A&A, 281, 817
Castelli, F., & Kurucz, R. L. 2003, in IAU Symp. 210, Modelling of Stellar Atmospheres, ed. N. Piskunov, W. W. Weiss, & D. F. Gray (San Francisco, CA: ASP), 20P
Chevalier, R. A. 2005, ApJ, 619, 839
Cordes, J. M., & Lazio, T. J. W. 2002, arXiv:astro-ph/0207156
Dale, J. E., & Bonnell, I. 2011, MNRAS, 414, 321
Dale, J. E., Ercolano, B., & Bonnell, I. A. 2012, MNRAS, 427, 2852
D'Alessio, P., Hartmann, L., Calvet, N., et al. 2005, ApJ, 621, 461
Draine, B. T. 2003, ARA&A, 41, 241
Gaensler, B. M., Arons, J., Kaspi, V. M., et al. 2002, ApJ, 569, 878
Hanson, M. M., Conti, P. S., & Rieke, M. J. 1996, ApJS, 107, 281
Hanson, M. M., Kudritzki, R.-P., Kenworthy, M. A., Puls, J., & Tokunaga, A. T. 2005, ApJS, 161, 154
Hanson, M. M., Rieke, G. H., & Luhman, K. L. 1998, AJ, 116, 1915
Heger, A., Fryer, C. L., Woosley, S. E., Langer, N., & Hartmann, D. H. 2003, ApJ, 591, 288
Herter, T. L., Henderson, C. P., Wilson, J. C., et al. 2008, Proc. SPIE, 7014, 30
Hillenbrand, L. A., Strom, S. E., Vrba, F. J., & Keene, J. 1992, ApJ, 397, 613
Koo, B.-C., McKee, C. F., Lee, J.-J., et al. 2008, ApJL, 673, L147
Koo, B.-C., Moon, D.-S., Lee, H.-G., Lee, J.-J., & Matthews, K. 2007, ApJ, 657, 308
Lang, C. C., Wang, Q. D., Lu, F., & Clubb, K. I. 2010, ApJ, 709, 1125
Leahy, D. A., Tian, W., & Wang, Q. D. 2008, AJ, 136, 1477
Lee, H.-G., Koo, B.-C., Moon, D.-S., et al. 2009, ApJ, 706, 441
Lee, J.-W., Koo, B.-C., & Lee, J.-E. 2012, JKAS, 45, 117
Lenorzer, A., Mokiem, M. R., de Koter, A., & Puls, J. 2004, A&A, 422, 275
Lu, F. J., Wang, Q. D., Aschenbach, B., Durouchoux, P., & Song, L. M. 2002, ApJL, 568, L49
Malfait, K., Bogaert, E., & Waelkens, C. 1998, A&A, 331, 211
Martins, F., Schaerer, D., & Hillier, D. J. 2005, A&A, 436, 1049
Meyer, M. R., Edwards, S., Hinkle, K. H., & Strom, S. E. 1998, ApJ, 508, 397
Monet, D. G., Levine, S. E., Canzian, B., et al. 2003, AJ, 125, 984
Moon, D.-S., Koo, B.-C., Lee, H.-G., et al. 2009, ApJL, 703, L81
Moon, D.-S., Lee, J.-J., Eikenberry, S. S., et al. 2004, ApJL, 610, L33
Salpeter, E. E. 1955, ApJ, 121, 161
Schmidt-Kaler, T. 1982, in Landolt–Börnstein, New Series, Group VI, Vol. 2, ed. K. Schaifers & H. H. Voigt (Berlin: Springer), 1
Skrutskie, M. F., Cutri, R. M., Stiening, R., et al. 2006, AJ, 131, 1163
Smith, N., Li, W., Filippenko, A. V., & Chornock, R. 2011, MNRAS, 412, 1522
Temim, T., Slane, P., Reynolds, S. P., Raymond, J. C., & Borkowski, K. J. 2010, ApJ, 710, 309
Velusamy, T., & Becker, R. H. 1988, AJ, 95, 1162
Wallace, L., & Hinkle, K. 1997, ApJS, 111, 445
Wallace, L., Meyer, M. R., Hinkle, K., & Edwards, S. 2000, ApJ, 535, 325
Weisskopf, M. C., Hester, J. J., Tennant, A. F., et al. 2000, ApJL, 536, L81
Wilson, J. C., Henderson, C. P., Herter, T. L., et al. 2004, Proc. SPIE, 5492, 1295
Zacharias, N., Monet, D. G., Levine, S. E., et al. 2004, BAAS, 36, 1418